C103-E156

SHIMADZU
Excellence in Science

FTIR TALK LETTER

Vol. 45

Kaikado, Kyoto—Celebrating 150 Years as Japan's Oldest Producer of Handmade Tea Canisters

Identification and Quantitation of Microscopic Elastomer Particles and Tire and Road Wear Particles (TRWPs) in Sediment Using a FTIR Microscopy Method

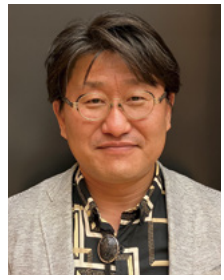

Department of Civil and Environmental Engineering, Faculty of Creative Engineering, Chiba Institute of Technology
Professor Yutaka Kameda

1. Introduction

In the early 2000s, a phenomenon termed urban runoff mortality syndrome (URMS) attracted significant attention following reports of abnormal behavior and mass die-offs of coho salmon (Oncorhynchus kisutch) in Puget Sound and lowland streams of Washington State, U.S.[1] Subsequent studies implicated as a major causal factor a transformation product of an antioxidant additive used in tires, N-(1,3-dimethylbutyl)-N-phenyl-p-phenylenediamine-quinone (6PPD-quinone, hereafter 6PPD-Q), generated by oxidative processes and which entered aquatic systems via tire wear particles (TWPs)[2]. These findings have underscored the importance of environmental monitoring of tire- and road-wear particles (TRWPs).

At present, one of the more accessible monitoring approaches employs Fourier transform infrared spectroscopy (FTIR) coupled with attenuated total reflection (ATR) to chemically identify and quantify black particles collected manually from road dust, surface waters, and sediments. However, this method inherently biases against particles smaller than 100 μm, while tire formulations vary substantially across manufacturers and production years, and reference spectral libraries remain incomplete. As a result, comprehensive assessments of TRWPs in environmental matrices remain challenging[3].

Pyrolysis–gas chromatography/mass spectrometry (Py-GC/MS) has been proposed as a more robust analytical technique, and has been published as a Technical Specification by the International Organization for Standardization (ISO)[4]. Yet, it has not been adopted as an International Standard. Concerns remain regarding the influence of sample impurities, carbon black content, particle size, and other factors on combustion efficiency and quantification accuracy. Moreover, oversimplified treatment of elastomer compositions across diverse tire types further undermines analytical precision[5, 6].

Addressing these challenges requires not only refinement of existing techniques but also the development and rigorous validation of complementary methods to achieve accurate environmental assessments of TRWPs. Given that 6PPD-Q is not unique to TRWPs and can also be derived from other synthetic elastomeric materials, environmental monitoring should logically be expanded to encompass elastomer particles more broadly.

Here, we present an FTIR microscopy-based method developed by the author to identify and quantify TRWPs as well as other elastomer particles ≥20 μm in sediments, and we discuss the methodological challenges and future perspectives of this approach.

2. Analytical Method for Microscopic Elastomer Particles and TRWPs in Sediment

(1) Overview and Sample Pretreatment

An overview of the analytical technique developed by this laboratory is shown in Figure 1. At present, this method can identify and quantitate the following 11 elastomer materials: chloroprene rubber (CR), chlorosulfonated polyethylene rubber (CSM), ethylene propylene rubber (EPR), tetrafluoroethylene propylene rubber (FEDM), butyl rubber (IIR), nitrile rubber (NBR), natural rubber (NR), polyurethane rubber (PU), silicone rubber (Q), styrene butadiene rubber (SBR), and fine particles derived from tires (TRWPs). An accurate analysis of particles of these elastomer materials in sediment requires a pretreatment process that removes all impurities other than these 11 materials. Unfortunately, a global standardized method of

preparing such samples has yet to be established. For this study, the findings[7] from a previously published method that was used to analyze microplastics 20 µm or larger were used to develop the following sample pretreatment method. The first step, which aims to remove organic impurities, uses potassium hydroxide and methanol in an alkali degradation step to decompose/pulverize organic substances into particles of 5 µm or smaller. Next, centrifugation with a high-density solution of sodium polytungstate is used to remove fine sand and other large inorganic particles with a high specific capacity that are present in the sediment. These sample pretreatment steps are undertaken in a single centrifugation tube to reduce the risk of contamination during analysis. In the final step of the pretreatment process, filtration was performed using a 5 µm pore silicon membrane, effectively removing impurities not relevant to the analysis. Figure 2 shows a microscopic image of the particles retained by the silicone membrane after sample pretreatment. The microscopic image shows well-distributed particles that do not overlap and almost all elastomer particles with very few impurities, demonstrating the efficacy of the sample pretreatment method. This sample was then subjected to imaging analysis by FTIR microscopy. Specifically, an aperture size of 30 × 30 µm, a step size of 15 µm, and a region measuring 2.5 × 5 mm were batch scanned, and the resulting IR spectra were compared against a spectral library to identify the elastomer particles in the scanned region.

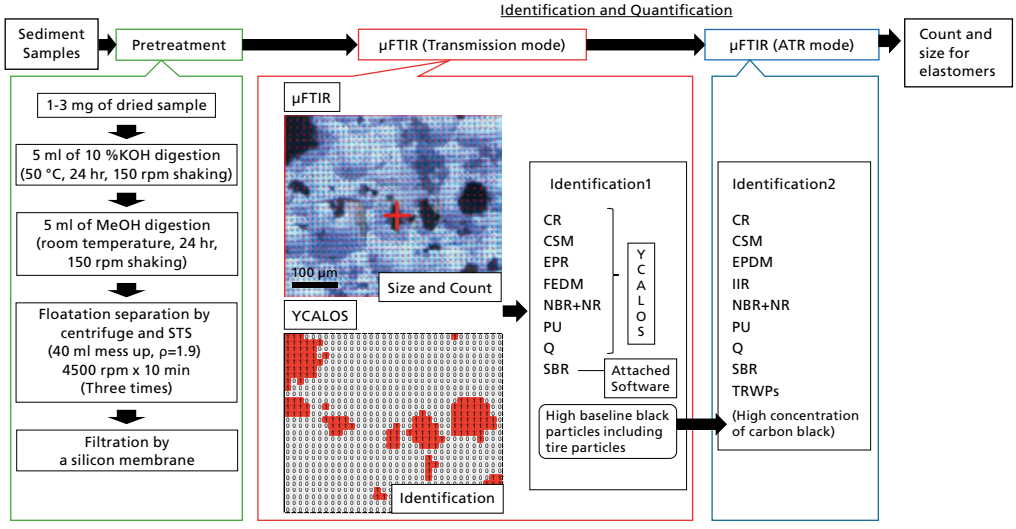

Figure 1: Overview of Analytical Technique Developed by this Laboratory for Elastomer Particles and Tire Particles 20 µm or Larger in Sediment

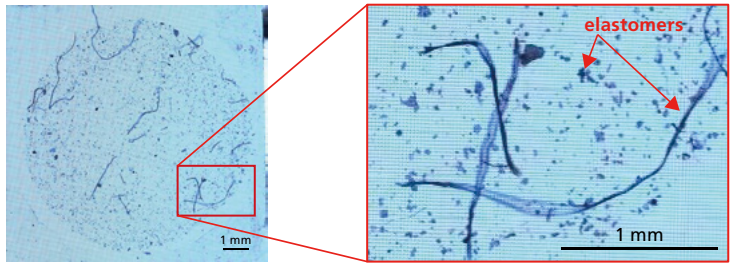

Figure 2: Microscopic Image of Processed Sediment Sample

(2) Creating a Spectral Library

Black colored elastomers and TRWPs typically contain a higher concentration of black carbon than other rubber products, which makes them unsuitable for analysis by transmission infrared spectroscopy. Instead, these materials are normally identified using the ATR method. As a result, IR spectral libraries obtained by the transmission method do not contain enough data to cross-reference the spectra of black elastomers and TRWPs. Transmission FTIR microscopy can rapidly analyze a wide target area and is an effective technique for the analysis of particles several tens of micrometers in size that are too small to be handled with tweezers. Given the advantages of transmission FTIR microscopy, this study attempted to build a reference spectral library compatible with transmission spectral measurements to identify microscopic

elastomer particles.

Reference spectra were obtained using rubber particles collected from a road near the laboratory and from the tread rubber of two automobile tires. These samples were first identified by ATR. They then underwent a pretreatment process consisting of freezing with liquid nitrogen and pulverization with a mortar after which transmission spectra were obtained by FTIR microscopy. As a result, elastomer-specific IR spectra were obtained from particles sized between 20 to 200 µm for eight types of elastomers, excluding those derived from tires and IIR (see Figure 3). Comparing these spectra against JIS-compliant reference transmission spectra[8] revealed a high degree of spectral similarity for some of the spectra but low spectral similarity for others. These results are likely due to compositional differences between environmental samples and standard materials, as well as degradation effects specific to environmental samples. Consequently, it became clear that collecting spectra from environmental samples is essential. The above findings showed that eight of the elastomer materials targeted in this study can be identified by the transmission method. Accordingly, the transmission spectra obtained above for these materials were used as reference spectra in the next part of this study. One point of note is that NBR exhibited IR spectra very similar to those of NR, because the characteristic peak attributed to the C≡N stretching vibration near 2240 cm^{-1} was not detected. For the purpose of this study, NBR and NR were not separated and are grouped together as NBR+NR. Given the global production levels of these two materials in 2022 (NR: around 14,570,000 tons, NBR: around 800,000 tons), it can be assumed the large majority of particles identified as NBR+NR are NR.

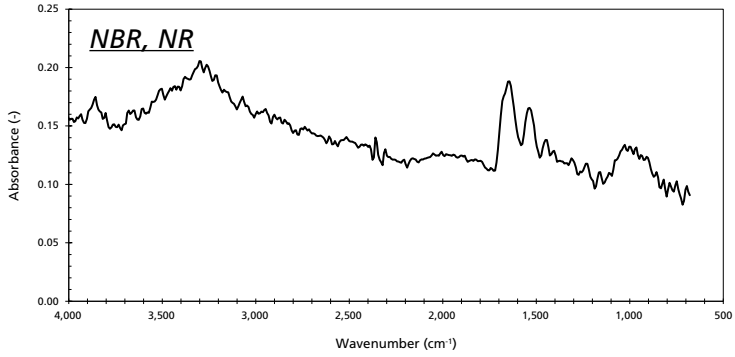

Figure 3: Transmission IR Spectra of Rubber Particles Collected from the Road (after Pulverization into Powder)

When powdered samples of automobile tire tread were analyzed by the transmission method, the spectral baseline increased by 0.1 or more, even when analyzing particles around 20 µm in size, and distinct absorption peaks were not readily detectable as shown in Figure 4. This poor spectral detection is believed to be caused by the high carbon black content of the tire tread samples. Accordingly, standard spectra could not be obtained by the transmission method. While previous reports have observed some differences between ATR IR spectra of tire samples based on year and producer[3], this study obtained consistent and reliable TRWP-specific ATR IR spectra from its samples. Based on the above findings, this study will identify TRWPs using standard IR spectra obtained by the ATR method and not standard IR spectra obtained by the transmission method.

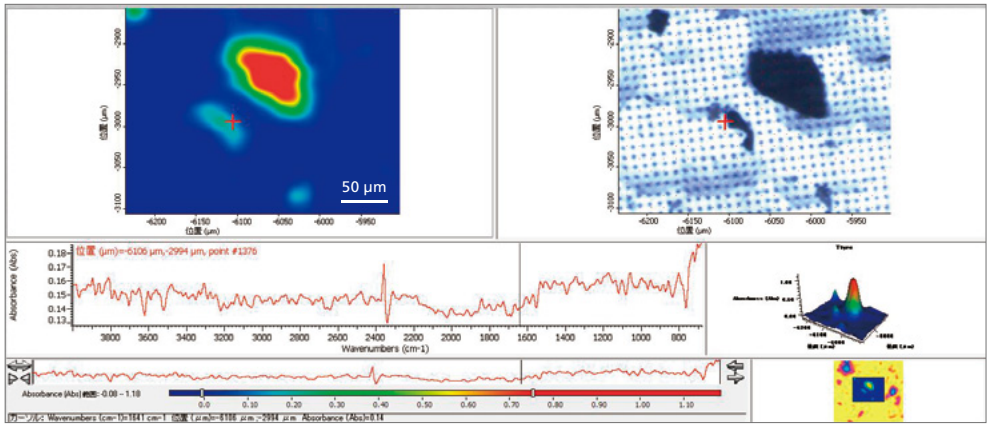

Figure 4: Microscopic Image and Transmission IR Spectrum of Tire Tread Particles Measuring Tens of Micrometers in Size

(3) Identification and Quantification with YCALOS

FTIR spectral-based identification of microplastics is typically performed using the hit quality index (HQI). However, microplastics and elastomer particles in the environment are often misidentified due to the presence of carbonyl absorption peaks associated with material degradation and overlapping peaks due to impurities coexisting in the sample. To avoid this misidentification, a check for absorption bands specific to each target material (key bands) and a visual inspection of the spectral profile must be introduced to the identification process in addition to quantitative HQI. This study aims to simplify this complex process by adapting an existing Excel macro designed to automatically identify microplastics (YCALOS [You CAn LOok for microplasticS]) for the identification of elastomer particles. YCALOS can use IR spectra obtained by FTIR microscopy in imaging or spot measurement modes, calculate the degree of similarity with reference spectra based on factors such as key polymer-specific absorption bands, relative intensity, and spectral profile, identify the target particle based on a user-specified level of accuracy, and create contour maps. YCALOS efficacy has been demonstrated in the identification of microplastics in environmental samples, where it identified 1 to 5 times as many detected particles as the conventional HQI-based software included with the equipment[9]. In this study, spectral data obtained by FTIR microscopy imaging were converted to the CSV format and input to YCALOS along with the previously-mentioned reference spectra. YCALOS was then used to generate contour diagrams of the elastomer particles. The contour diagrams were analyzed by ImageJ software to quantify the number of particles and the particle size distribution. Some of the black particles produced no distinct absorption peaks and could not be identified by YCALOS. For all these particles, the baseline of the transmittance spectrum was raised by at least 0.1. This raised baseline was assumed to be caused by light absorption by TRWPs with a high carbon black content or due to saturation caused by particle thickness. To verify these assumptions, the black particles in question were analyzed by ATR FTIR microscopy, whereupon the resulting spectral measurements confirmed the particles were either TRWPs or elastomer particles whose spectral features were affected by sample thickness.

One point of note is that the characteristic key band for SBR is broad and of low intensity, and identifying SBR with YCALOS alone may give less accurate results than for other elastomer materials. Accordingly, SBR was identified by a combination of YCALOS and the standard software included with the FTIR system.

Based on the above findings, elastomer particles 20 µm or larger were identified by the following two-step process. First, imaging FTIR microscopy measurements, YCALOS, and the software included with the equipment were used to prepare contour diagrams and calculate the number of particles and particle sizes for eight types of elastomer particles (excluding TRWPs and IIR) and for potential TRWP particles with a raised baseline (nine types of particles in total). Next, the potential TRWP particles were analyzed again by the ATR method and the elastomer material was identified based on these IR spectra.

(4) Analysis of Sediment from Tokyo Bay

The method described above was used to analyze samples of surface sediment collected from the middle of Tokyo Bay. As shown in Figure 5, 1.70×10^5 elastomer particles were detected per gram of dried sediment. The most common particles detected were NR+NBR particles (63.1 %), followed by IIR (14.8 %), and SBR (10.7 %). These three materials accounted for 88.6 % of all particles. IIR, SBR, and EPDM accounted for the highest proportion of synthetic rubber particles in that order, where the order of their prevalence reflected the amounts of these same synthetic rubbers shipped domestically in Japan[10]. The estimated concentration of TRWPs in Tokyo Bay sediment based on this analysis was 9.8 % of all targeted particles. The results of this study cannot be compared directly with previous studies, as prior research into the composition and concentration of elastomer particles and TRWPs in Tokyo Bay is very limited. Instead, using the number and long and short diameters of particles recorded in this study, and assuming a particle thickness of 20 µm, masses were calculated based on particle volumes and known material densities and compared with similar results obtained from Py-GC/MS analysis of sediment from Yodo River and Biwa Lake in Japan[11]. The total mass of all elastomer particles in Tokyo Bay sediment was estimated at 9,860 µg/g of dry sediment, which was higher than the maximum and mean levels of TRWPs in sediment from Yodo River and Biwa Lake by Py-GC/MS (4,600 and 770 µg/g of dry sediment, respectively). The estimated concentration of TRWPs alone in Tokyo Bay sediment was 1,770 µg/g of dry sediment, which was within the range of concentrations determined by previous reports. This study uses a method that measures all elastomer polymers and not just TRWPs. For this reason, this study detected a higher overall concentration of elastomer materials in sediment compared to previous studies. However, limiting this analysis to only TRWPs gives results consistent with previous studies. These findings indicate the analytical method described in this article provides results consistent with previous

studies while also offering a more comprehensive dataset. Furthermore, assuming these results are correct, it is possible that high concentrations of elastomers with a low carbon black content, likely not derived from TRWPs, are present and may lead to a positive bias in TRWPs estimates based on Py-GC/MS.

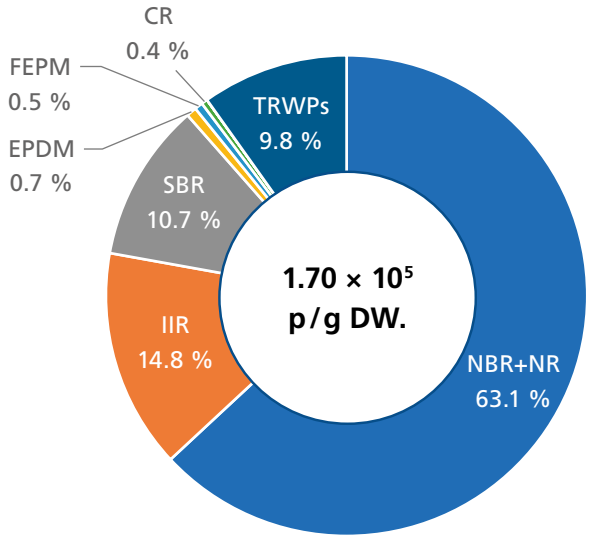

Figure 5: Concentration and Composition of Elastomer Particles in Sediment from the Center of Tokyo Bay

Furthermore, as shown in Figure 6, 45.8 µm was the medium elastomer particle size according to the particle size distribution measured by this method, which is substantially smaller than the particles measured by most previous studies. A comparative study that analyzes the same samples by Py-GC/MS and the method presented in this study is needed to obtain insights into the relative limitations of the two methods and how the methods complement each other.

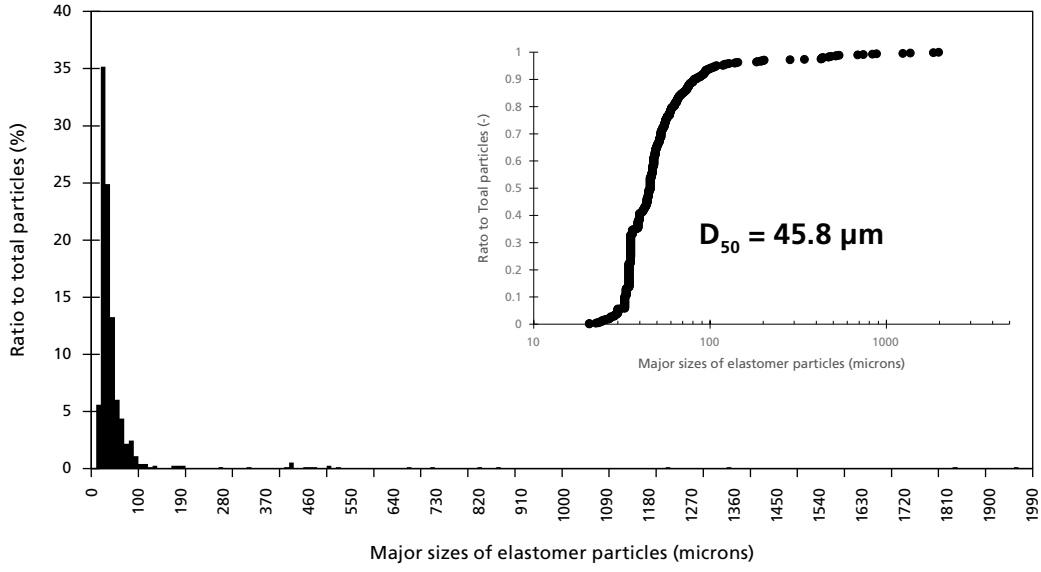

Figure 6: Size Distribution of Elastomer Particles in Sediment from the Center of Tokyo Bay

3. Conclusion

This article describes an analytical method that differs from existing methods and prior approaches by using transmission FTIR microscopy to identify and quantify microscopic elastomer particles. Although the transmission method has typically been considered unsuitable for the analysis of black particles, this transmission-based analytical method allowed for successfully analyzing over 90 % of all black particles found in Tokyo Bay sediment.

The reason for this success was verified by microscopic imaging that showed the black particles in sediment were thin enough to appear gray and allow transmission of visible and infrared light. Nevertheless, the transmission method is still likely to be unsuitable for cases such as road runoff samples collected during rainfall because they will probably contain large numbers of thick, spherical particles.

This analytical method also requires a highly accurate spectral library that covers the targeted elastomers, as well as software equipped with a very reliable identification algorithm. Despite this, the method described in this article has a relatively simple sample pretreatment and measurement process, and may be suitable for atmospheric samples as well as environmental water samples.

In the future, this method will be applied not only to environmental water samples, including sewer water, road dust, sediments, and biological samples, but also to airborne particles. Through these applications, the limitations and issues of the method will arise, and improvements will be made as necessary, with the aim of establishing a general-purpose method for the analysis of elastomer particles in the environment.

References

[1] Scholz, N.L., Myers, M.S., McCarthy, S.G., Labenia, J.S., McIntyre, J.K., Ylitalo, G.M., Rhodes. L.D., Laetz, C.A., Stehr, C.M., French, B.L., McMillan, B., Wilson, D., Reed, L., Lynch, K.D., Damm, S., Davis, J.W., Collier, T.K., Recurrent Die-Offs of Adult Coho Salmon Returning to Spawn in Puget Sound Lowland Urban Streams, *PLoS ONE*, 2011, **6**, e2803.

[2] Tian, Z., Zhao, H., Peter, K.T., Gonzale, M., Wetzel, J., Wu C., Hu, X., Prat, J., Mudrock, E., Hettinger R., Cortina, A.E., Ghosh Biswas, R.G., Kock, F.V.C., Soong, R., Jenne, A., Bowen Du, B., Hou, F., He, H., Lundeen, R., Gilbreath, A., Sutton, R., Scholz, N.L., Davis, J.W., Dodd, M.C., Simpson, A., McIntyre, J.K., Kolodziej, E.P., A ubiquitous tire rubber–derived chemical induces acute mortality in coho salmon, 2020, *Science*, **371**, 185-189.

[3] Kanako Yamamoto and Hiroaki Furumai, "Method for Identification of Black Microplastics by Using Tire Library with ATR-FTIR Analysis," *Journal of Japan Society of Civil Engineers*, G, 2022, **78**, III-349–III-358.

[4] ISO, 2017b. ISO/TS 20596:2017b. Rubber–Determination of Mass Concentration of Tire and road Wear Particles (TRWP) in Soil and Sediments – Pyrolysis-GC-MS Method (Switzerland).

[5] Jeong, S., Ryu, H., Kim, H., Shin, H., Kwon, J.T., Lee, M.G., Lee, J., Hong, J., Kim, Y., Quantification of tire wear particles in road dust based on synthetic/natural rubber ratio using pyrolysis-gas chromatography–mass spectrometry across diverse tire types, 2024, *STOTEN*, **942**, 173796.

[6] Rauert, C., Rødland, E.S., Okoffo, E.D., Reid, M.J., Meland, S., Thomas, K.V., Challenges with Quantifying Tire Road Wear Particles: Recognizing the Need for Further Refinement of the ISO Technical Specification, 2021, *Environ. Sci. Technol. Lett.*, **8**, 231-236.

[7] Kameda, Y., Yamada, N., Fujita, E., Source- and polymer-specific size distributions of fine microplastics in surface water in an urban river, 2021, *Environ. Pollut.*, **284**, 117516.

[8] Japanese Industrial Standards (JIS) 2018. K6230 Rubber—Identification—Infrared spectrometric methods, https://kikakurui.com/k6/K6230-2018-01.html (1. As of July 2025)

[9] Shingo Rachi, Yutaka Kameda, and Emiko Fujita, "Development of an automated identification and quantification software for environmental microplastics analysis," 2022, Proceedings from 56th Annual Meeting of Japan Society on Water Environment, 460.

[10] Japan Rubber Manufacturers Association (JRMA), Statistics on rubber products, https://www.rubber.or.jp/page3.html?id=6 (as of July 2025)

[11] Unice, K.M., Kreider, M.K., Panko, J.M., Comparison of Tire and Road Wear Particles Concentrations in Sediment for Watersheds in France, Japan, and the United States by Quantitative Pyrolysis GC/MS Analysis, 2013, *Environ. Sci. Technol.*, **47**, 8138-8147.

The IRSpirit-ZX FTIR Spectrophotometer

Spectroscopy Business Unit, Analytical & Measuring Instruments Division
Ayato Kuroki

1. Introduction

In December 2023, Shimadzu launched the IRSpirit-X series FTIR spectrophotometers as its next generation of compact IRSpirit FTIR systems. The IRSpirit-X series includes the smallest and lightest FTIR spectrophotometers ever produced by Shimadzu, with a footprint of 420 × 297 mm (an A3-sized piece of paper) and a weight of just 8.5 kg. The IRSpirit-X series also offers class-leading sensitivity (S/N of 37,000:1 measured for IRSpirit-TX with KBr window) among compact FTIR spectrophotometers. The IRSpirit-X series features a sample chamber the same width as high-end models and can accommodate a range of FTIR accessories (including Shimadzu and third-party accessories), offering users excellent expandability in a compact package.

The IRSpirit-X series comes equipped with powerful tools to help analysts: the IR Pilot program that navigates users through an analysis via interactive prompts, and the Spectral Advisor feature that compares spectral measurements with examples and suggests improvements. All non-consumable components in the IRSpirit-X series are also guaranteed for 10 years (labor costs not included in parts replacement).

The IRSpirit-X series comes in three models that vary by detector type and level of moisture resistance: the IRSpirit-TX, IRSpirit-LX, and IRSpirit-ZX. The IRSpirit-TX and IRSpirit-LX use different detectors. The differences between these detectors are outlined in FTIR TALK LETTER Vol. 31.

IRSpirit-ZX is new to the IRSpirit-X series lineup and equipped with a zinc selenide (ZnSe) beam splitter. A key feature of IRSpirit-ZX is its moisture resistance, being designed for use in high-temperature and high-humidity environments. Unlike the potassium bromide (KBr) beam splitter found in the IRSpirit-TX and IRSpirit-LX, the ZnSe beam splitter in the IRSpirit-ZX is hardly deliquescent. Therefore, when using IRSpirit-ZX, this removes any concerns about performance degradation when the dehumidifying agent is not replaced (corrosive components in the environment can react with ZnSe and reduce its transmission; hence, silica gel is used to physically absorb these corrosive components and must be replaced every three months). The IRSpirit-X series offers a variety of options for the beam splitter, detector, and window, providing a high level of flexibility to meet the demands of the operating environment and analytical objectives. The specifications of each model in the IRSpirit-X series are shown below.

Table 1: Comparison of IRSpirit-X Series Models

	IRSpirit-TX	IRSpirit-LX	IRSpirit-ZX
Beam Splitter	KBr	KBr	ZnSe
Detector	DLATGS	$LiTaO_3$	DLATGS
Window	KBr or KRS-5	KBr or KRS-5	KRS-5
Wavenumber Range	7,800 to 350 cm^{-1}	7,800 to 350 cm^{-1}	6,000 to 550 cm^{-1}

2. Zinc Selenide (ZnSe)

This section describes ZnSe, the material used as the beam splitter in IRSpirit-ZX. ZnSe is a common material for optical applications. Due to its excellent transmission of infrared light, it is often used in thermography, window plates for CO_2 lasers, infrared lenses, and prisms. Compared to KBr, ZnSe has a narrower infrared transmission range, but it is hardly deliquescent. Deliquescency is a phenomenon during which atmospheric moisture condenses on the surface of the substance, causing it to dissolve and form an aqueous solution. The IRSpirit-TX and IRSpirit-LX use a KBr beam splitter that is highly deliquescent.

The following demonstrates the effect of deliquescence on a KBr window. Figure 1 shows a KBr window after two weeks in a high-temperature and high-humidity environment at 40 °C and 70 % humidity. Deliquescence of the KBr crystal has caused the originally transparent KBr window to change to cloudy white. Figure 2 shows the difference in transmittance between a normal KBr window and a KBr after deliquescence, demonstrating that deliquescence reduces the transmittance of infrared light (and higher wavenumbers in particular) through the KBr window.

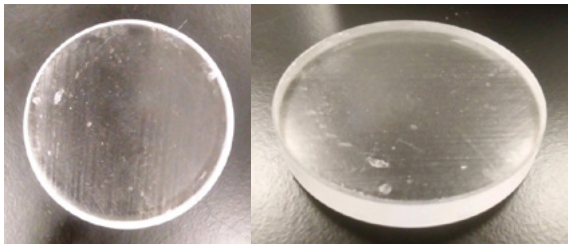

Figure 1: KBr Crystal after Deliquescence

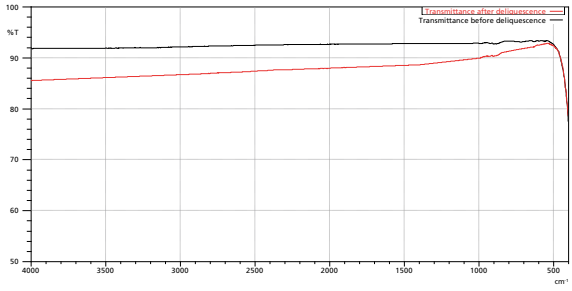

Figure 2: Transmittance of a KBr Window before/after Deliquescence
(Black line: Normal KBr window; Red line: KBr window after deliquescence)

Figure 3 shows the change in infrared intensity (power spectrum) at 700 cm^{-1} and 4,000 cm^{-1} at one-week intervals after a KBr beam splitter was placed in the same environment. The results in Figure 3 show that deliquescence has a greater effect on higher wavenumbers, causing a greater change in infrared intensity at the higher wavenumber (4,000 cm^{-1}) than the lower wavenumber (700 cm^{-1}). This change in infrared intensity is caused by scattering of infrared light at the surface of the KBr crystal following deliquescence. The effect on infrared intensity is greater at higher wavenumbers because higher wavenumbers are more susceptible to light scattering. As shown in Figure 3, the longer a KBr beam splitter remains in a high-temperature and high-humidity environment, the lower the infrared intensity, and the greater the impact on accuracy. ZnSe does not undergo this deliquescence.

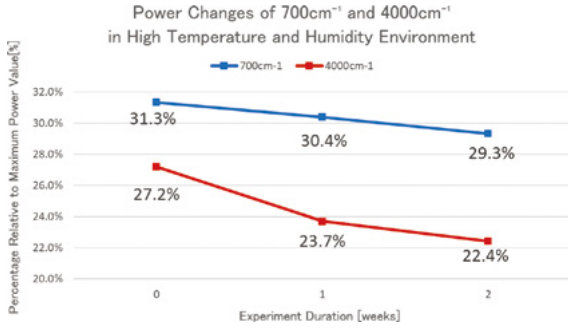

Figure 3: Changes in Infrared Intensity at 700 cm^{-1} and 4,000 cm^{-1} during the High-Temperature and High-Humidity Experiment

As noted in Table 1, KBr and ZnSe have different transmission ranges. Figure 4 compares the transmittance of the KBr and ZnSe used by Shimadzu and shows KBr has a wider transmission range than ZnSe. In light of these attributes, we recommend using IRSpirit-ZX for applications where moisture resistance is important and a broad transmission range is not required.

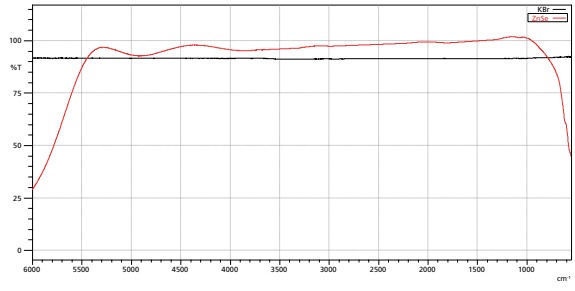

Figure 4: Transmittance of KBr and ZnSe
(Black line: KBr; Red line: ZnSe)

3. Experimental Comparison Between KBr and ZnSe

This section uses IRSpirit-TX and IRSpirit-ZX to perform transmission measurements of the same sample and look for differences in the acquired data. Commercially available plastic bags (polyethylene) were analyzed by single reflection ATR using the QATR-S ATR attachment designed specifically for IRSpirit systems. A photograph of the plastic bags is shown in Figure 5.

The analytical conditions used are shown in Table 2, and the measurements taken are shown in Figures 6 and 7.

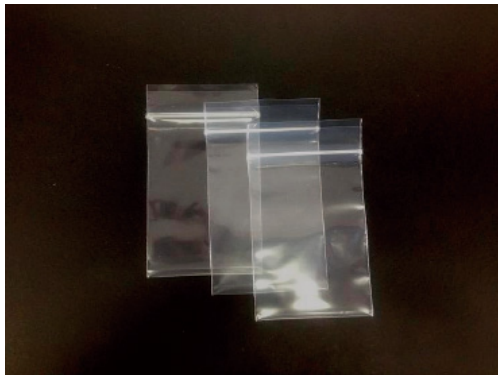

Figure 5: Plastic Bags

Table 2: Analytical Conditions

Instrument	IRSpirit-TX/IRSpirit-ZX
Window	KRS-5
Resolution	4.0 cm^{-1}
Number of Averaged Scans	20
Apodization Function	Square-Triangle
Attachment	QATR-S (Prism: diamond)

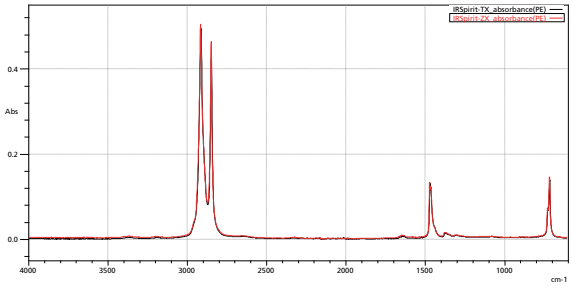

Figure 6: ATR Spectrum of Plastic Bag
(Black line: IRSpirit-TX; Red line: IRSpirit-ZX)

Figure 6 shows no major difference between the measured spectra and the polyethylene absorption peaks detected by both models. Figure 7 shows an expanded view of Figure 6 limited to a wavenumber range that is unaffected by atmospheric water vapor or carbon dioxide (1,200 to 600 cm^{-1}).

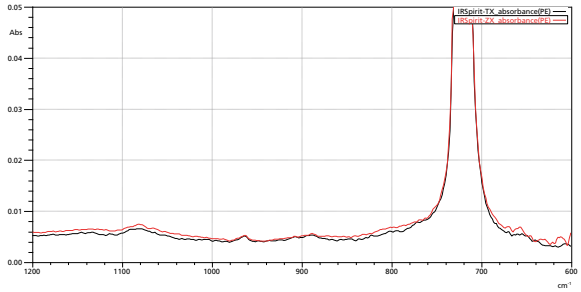

Figure 7: Expanded View of Figure 6 from 1,200 to 600 cm^{-1}
(Black line: IRSpirit-TX; Red line: IRSpirit-ZX)

Figure 7 also shows no major difference between the measured spectra, but it reveals that noise is slightly more visible at lower wavenumbers (700 to 600 cm^{-1}) with IRSpirit-ZX. This is because the cutoff wavenumber for IRSpirit-ZX is 550 cm^{-1}, which results in lower power between the 700 and 600 cm^{-1} range and significant noise in the absorbance spectrum. These results show that both models are equally capable of qualitative analysis across wavenumbers that do not include cutoff wavenumbers.

4. Conclusion

This paper describes the characteristics of IRSpirit-ZX, a new model in Shimadzu's IRSpirit-X series, and some differences compared to other models in the IRSpirit-X series. Key features of the IRSpirit-ZX are its reliability in hot and humid conditions and its high sensitivity. This article is intended to help customers select the right model from the IRSpirit-X series. We hope you will have the opportunity to use the IRSpirit-ZX.

Notes on Infrared Spectral Analysis —Carbonyls (Part 2)—

Solutions COE, Analytical & Measuring Instruments Division
Yoshiyuki Tange

1. Introduction

The previous issue (FTIR TALK LETTER Vol. 44) discussed the peak positions of C=O stretching vibrations in several molecules that include carbonyl groups. The position of peaks from C=O stretching vibration can shift due to structures or atoms adjacent to the carbonyl group, and the previous issue described the specific causes of these shifts. These included the mass of adjacent structures, bond angles, inductive effects, and mesomeric effects. This article (Part 2) on carbonyls discusses methods of infrared spectral analysis using peaks other than those associated with C=O stretching vibrations.

2. Classifying Carbonyl Groups by Infrared Spectra

Figure 1 shows the position of key peaks in the infrared spectrum of a compound with carbonyl groups and how to classify those peaks. As well as the peak in the 1,780 to 1,650 cm^{-1} region associated with C=O stretching vibrations, carboxylic acids, esters, ketones, and aldehydes can all be classified based on the presence of various other characteristic peaks.

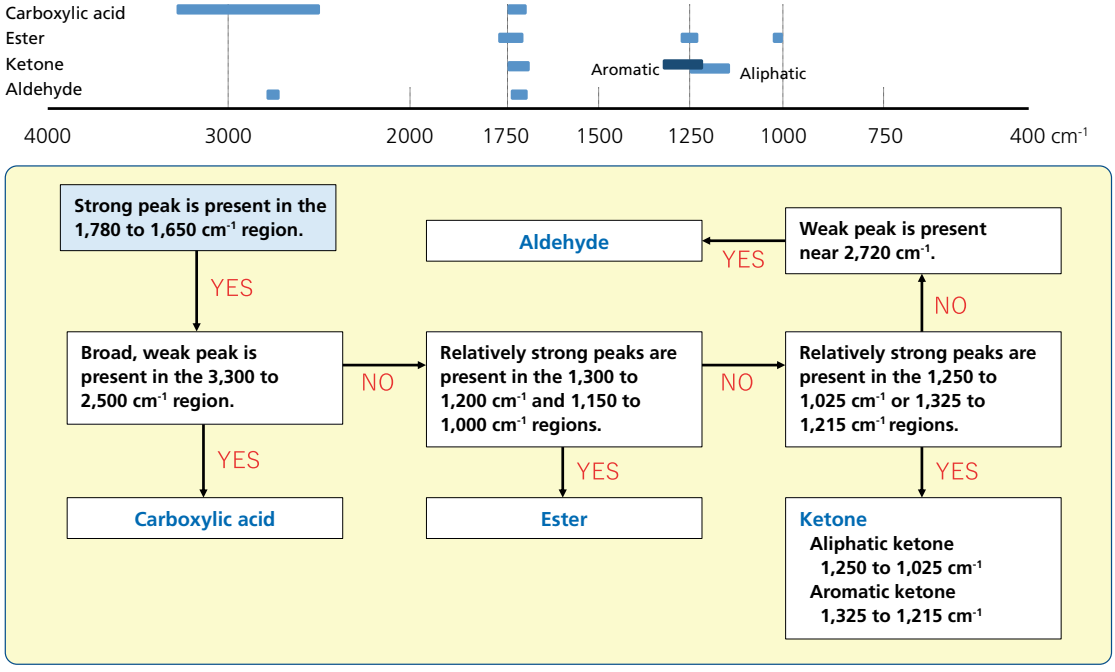

Figure 1: IR Spectral Peak Positions and Classification Flowchart for Carbonyls

(1) Identifying Carboxylic Acid: Broad, Weak Peak in the 3,300 to 2,500 cm^{-1} Region

The hydroxyl group in carboxylic acid forms a hydrogen bond with the carbonyl group of another carboxylic acid, creating a ring dimer. Because of the weakness of the bond with OH, the broad OH-stretching vibration that is normally centered at 3,500 cm^{-1} stretches toward lower wavenumbers, creating a broad peak in the 3,300 to 2,500 cm^{-1} region. The position of the peak associated with the carbonyl group also shifts due to the presence of adjacent functional groups. Carboxylic acids can be identified based on this carbonyl group peak and a hydroxyl group peak that is broadly shifted toward lower wavenumbers.

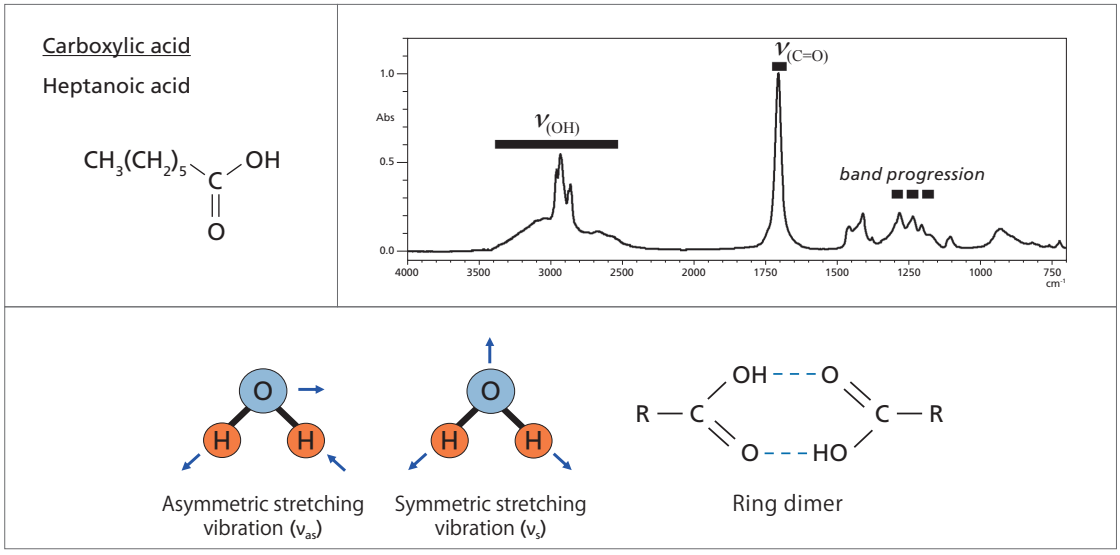

Figure 2: Infrared Spectrum of Heptanoic Acid and Attribution of a Broad, Weak Peak in the 3,300 to 2,500 cm^{-1} Region

Solid fatty acids produce characteristic regularly spaced weak peaks in the 1,350 to 1,180 cm^{-1} region. These peaks are called band progressions and can be used to estimate the length of the methylene chain. When the n in $(CH_2)n$ is an even number, there are n/2 bands, and when the n is odd, there are (n+1)/2 bands[1, 2]. Figure 3 shows the infrared spectra for stearic acid and lauric acid. The band progressions are relatively weak peaks, and the transmittance is plotted on the vertical axis for clearer visualization. Stearic acid has 8 band progressions because n = 16, and lauric acid has 5 band progressions because n = 10. As well as carboxylic acid, band progressions appear with carboxylates, long chain fatty acid esters, and long chain aliphatic amides, among other compounds. At present, a gas chromatograph (GC) is most commonly used for this type of analysis.

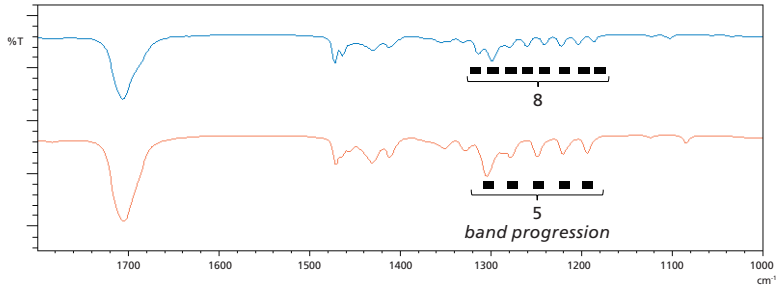

Figure 3: Infrared Spectra of Stearic Acid (Blue) and Lauric Acid (Orange) (Vertical Axis: Transmittance)

(2) Identifying Esters: Relatively Strong Peaks in the 1,300 to 1,200 cm^{-1} and 1,150 to 1,000 cm^{-1} Regions

The C-O-C stretching vibrations in esters appear as two strong peaks in the above wavenumber regions. The higher wavenumber peak is associated with C-O-C asymmetric stretching vibrations, and the lower wavenumber peak is associated with C-O-C symmetric stretching vibrations. Because the intensity of the peak associated with the C-O-C asymmetric stretching vibration is comparable to that for the C=O stretching vibration, this peak can be used to distinguish esters from other carbonyl compounds.

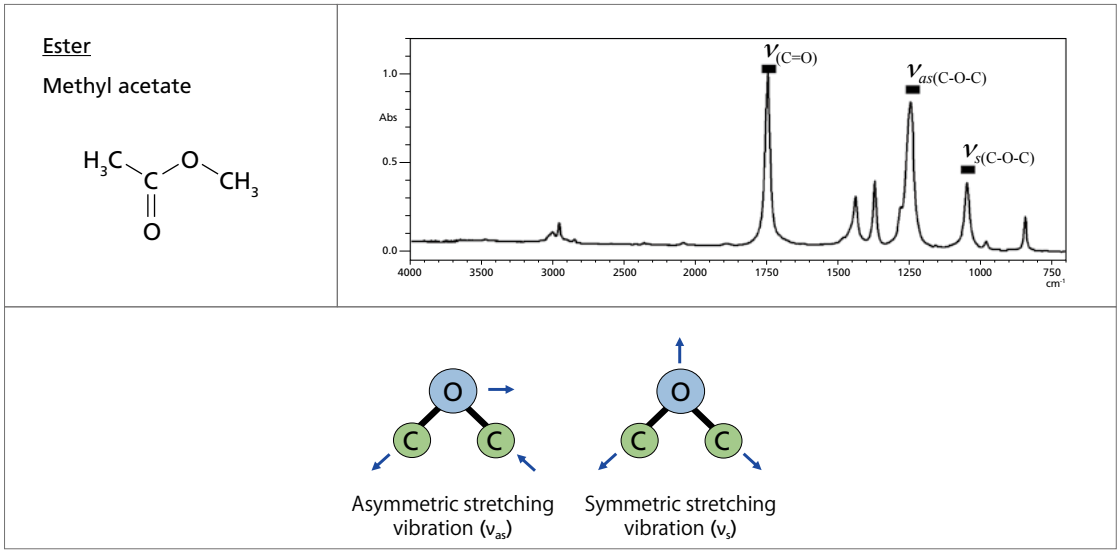

Figure 4: Infrared Spectra of Methyl Acetate and Attribution of Relatively Strong Peaks in the 1,300 to 1,200 cm^{-1} and 1,150 to 1,000 cm^{-1} Regions

(3) Identifying Ketones: Relatively Strong Peak in the 1,250 to 1,025 cm^{-1} or 1,325 to 1,215 cm^{-1} Region

The wavenumber band peak that can be used to identify ketones is attributed to the C-C-C asymmetrical stretching vibration. This peak appears in the 1,250 to 1,025 cm^{-1} region for aliphatic ketones and the 1,325 to 1,215 cm^{-1} region for aromatic ketones. Aromatic ketones are a conjugate system (continuous chain of double and single bonds) between a phenyl group and a carbonyl group. The peak is shifted to a higher wavenumber compared to aliphatic ketones because of the stronger C-C-C bond.

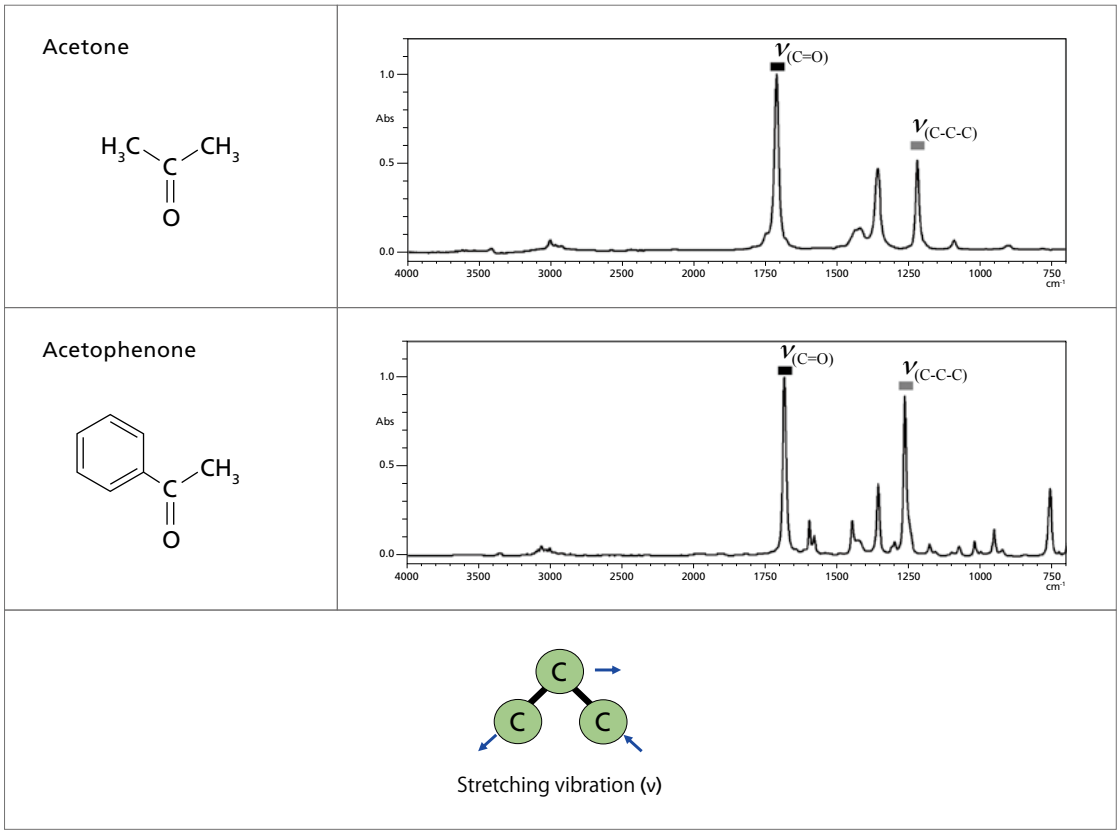

Figure 5: Infrared Spectra of Acetophenone and Acetone and Attribution of a Relatively Strong Peak in the 1,250 to 1,025 cm^{-1} or 1,325 to 1,215 cm^{-1} Region

(4) Identifying Aldehydes: A Weak Peak at 2,720 cm^{-1}

A peak around 2,720 cm^{-1}, attributed to Fermi resonance, can be used to identify aldehydes. Fermi resonance occurs when the combination tone or overtone of a given molecular vibration is close to the fundamental tone (≈ fundamental vibration) of another molecular vibration. Resonance between the two vibrations causes the single fundamental vibration to split into two peaks[3]. In theory, the peak splits into two peaks equidistant from the wavenumber position of the fundamental vibration. In the case of aldehydes, the CH stretching vibration and an overtone of the CH scissoring vibration (1,400 cm^{-1}) appear at almost the same wavenumber, 2800 cm^{-1}. This creates the conditions for Fermi resonance and causes the single peak to split into two peaks. Although not equidistant from 2,800 cm^{-1}, two peaks appear at characteristic wavenumbers of 2,820 cm^{-1} and 2,720 cm^{-1}. Figure 6 shows the infrared spectrum of acetaldehyde and an energy diagram explaining Fermi resonance.

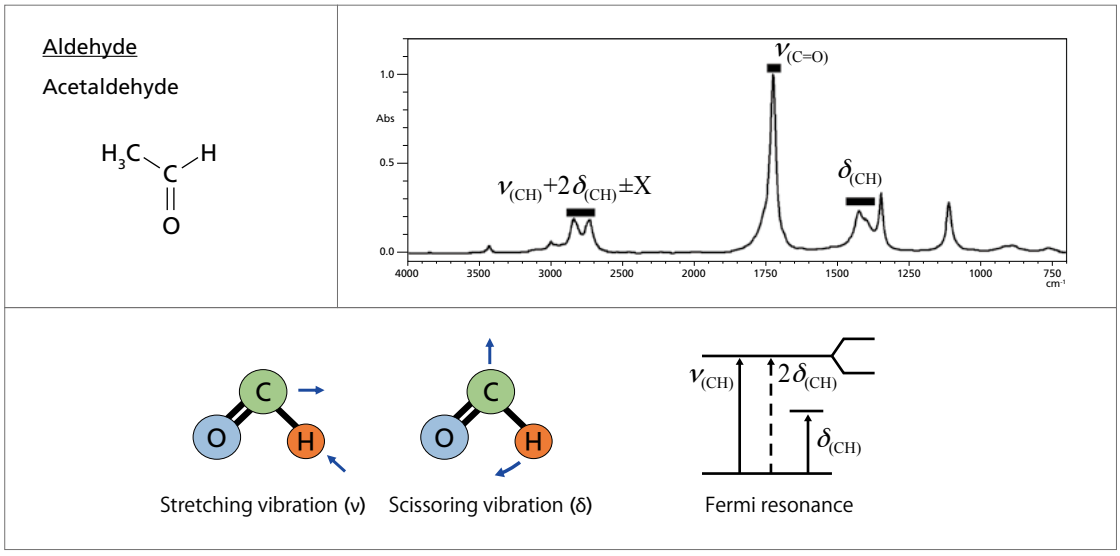

Figure 6: Infrared Spectrum of Acetaldehyde and Attribution of the Weak Peak Near 2,720 cm^{-1}

3. Applications

Fatty acid methyl esters (FAMEs) are already being used in carbon-neutral fuel. Waste cooking oil can be combined with diesel oil as fuel for automobiles, but cooking oil without pretreatment causes problems for automobile engines due to its high viscosity. This issue is resolved by reacting the waste cooking oil with a catalyst to create methyl esters and adding this to diesel oil as FAMEs.

The amount of FAMEs added to diesel oil can be quantified by measuring the height of the peak associated with the C=O stretching vibration. The C=O stretching vibration peak increases in size according to FAME concentration because the main component of diesel is saturated hydrocarbons, which do not interfere with this peak. Figure 7 shows the infrared spectrum of a FAME standard solution (FAME37). The strong peak near 1,750 cm^{-1} is associated with the C=O stretching vibration.

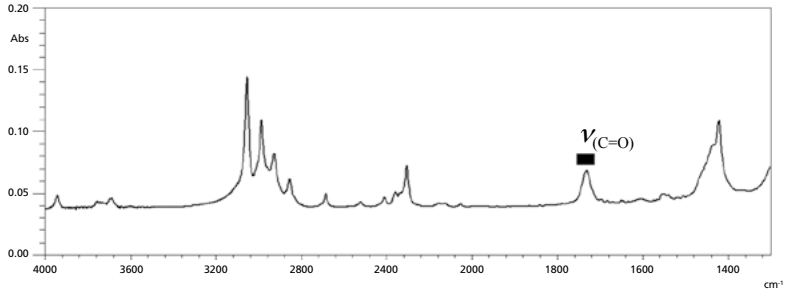

Figure 7: Infrared Spectrum of FAME37 Standard Solution (Dichloroethane Solvent)

For details of the quantitative analysis of FAMEs by FTIR, refer to Application News No. A600 "Quantitative Analysis of FAME (Fatty Acid Methyl Ester) in Diesel Fuel by FTIR."

4. Conclusion

This article discusses how to identify several molecules that include carbonyl groups.

- Carboxylic acids can be identified by looking for a broad, weak peak in the 3,300 to 2,500 cm^{-1} region associated with the OH stretching vibration.
- Esters can be identified by looking for relatively strong peaks in the 1,300 to 1,200 cm^{-1} and 1,150 to 1,000 cm^{-1} regions associated with the C-O-C stretching vibration.
- Ketones can be identified by looking for a relatively strong peak in the 1,250 to 1,025 cm^{-1} or 1,325 to 1,215 cm^{-1} region associated with the C-C-C asymmetric stretching vibration.
- Aldehydes can be identified by looking for a weak peak at 2,720 cm^{-1}. This peak is caused by Fermi resonance between the CH stretching vibration and an overtone of the CH bending vibration.

This article also noted the multiple peaks (band progressions) that appear depending on the number of methylene groups in a carboxylic acid, and the infrared spectra of FAMEs used as environmentally friendly non-fossil fuels.
The next issue will cover practical methods of analyzing the infrared spectra of some of the more characteristic amides that contain carbonyl groups.

References

[1] Shigeyuki Tanaka, Norio Teramae, *Infrared Spectroscopy*, Kyoritsu Shuppan (1993)

[2] Yukio Furukawa, *Infrared Spectroscopy*, Kodansha Scientific (2018)

[3] Larkin P.J. Infrared and Raman Spectroscopy: Principles and Spectral Interpretation, Elsevier (2011)

AIMsight Infrared Microscope & AIRsight Infrared/Raman Microscope

New Function

No liquid nitrogen required!

New detector capable of infrared microscopy measurements of minute samples.

New Option
TEC MCT (Peltier Cooled MCT) Detector

Equipping the AIMsight Infrared Microscope or the AIRsight Infrared/Raman Microscope with the TEC MCT (peltier cooled MCT) detector makes it possible to obtain infrared spectra without using liquid nitrogen. If more sensitivity is required, simply switch to the standard T2SL*1 detector in the software.

*1: Liquid nitrogen is required when using the T2SL.

IRXross Fourier Transform Infrared Spectrophotometer
AIRsight™ Infrared/Raman Microscope

Highlights of the Three Detectors

Choose the optimal detector for the application. The T2SL*2 detector is ideal for measuring microscopic areas 25 µm in size or smaller. A room temperature detector (DLATGS)*3, *4 is also available for acquiring data with a wavenumber range up to 400 cm^{-1}.

Detector	**T2SL** *2	**TEC MCT** *3	**DLATGS** *3,*4
Standard/Optional	Standard	Optional	Optional
Suitable Measurement Size	10 × 10 µm or larger	25 × 25 µm or larger	100 × 100 µm or larger *5
Liquid Nitrogen	Required	Not required	Not required
Measured Wavenumber Range	5,000 to 700 cm^{-1}	5,000 to 700 cm^{-1}	4,600 to 400 cm^{-1}

*2: Liquid nitrogen is required when using the T2SL.
*3: A TEC MCT and DLATGS cannot be installed at the same time.
*4: The DLATGS can measure across a wide wavenumber range. However, its sensitivity is substantially lower than the T2SL and TEC MCT.
*5: Measurable size in transmission/reflection method.

Examples of Analyses Using the TEC MCT (Peltier Cooled MCT) Detector

Infrared spectra of polypropylene-based (containing TALC) resin for automotive bumpers are shown to the right to compare the three detectors. The sample was placed in a diamond cell and measured in transmission method. It was measured by the T2SL and **TEC MCT** with a 25 × 25 µm aperture size, and by the DLATGS with a 100 × 100 µm aperture size. Liquid nitrogen was not used with the **TEC MCT**, and it is evident that there is a little more noise in the spectrum collected with the T2SL, which does require liquid nitrogen. A larger aperture is needed for data collection with the DLATGS detector due to its much lower sensitivity than the T2SL and **TEC MCT**. However, the DLATGS does have the advantage of being able to measure the sample in the low wavenumber region (down to 400 cm^{-1}).

In addition to the transmission method, analysis can be performed by the reflection method and ATR method (optional).

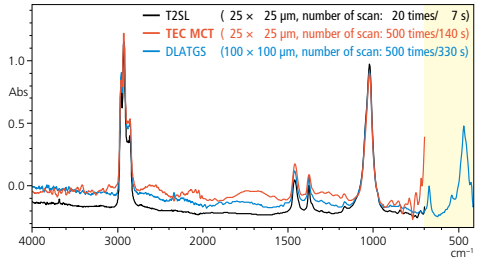

SHIMADZU

Shimadzu Corporation
www.shimadzu.com/an/